

COVERING A SPHERE WITH RETROREFLECTORS

Daniel Clouse
Carl Christian Liebe
Curtis Padgett
Randall Bartman

Jet Propulsion Laboratory, California Institute of Technology,
4800 Oak Grove Dr, Pasadena CA 91109-8099.
daniel.clouse@jpl.nasa.gov

Abstract- One of the future missions for Mars involves returning a soil sample from the Martian surface to Earth. The sample will be deposited in a spherical canister, shot into Mar's orbit and then subsequently captured by a spacecraft for the return journey. This paper discusses how retroreflectors can be placed on the orbiting sample canister with the objective of maximizing returned light from a scanning laser system. The retroreflectors are vital for acquisition of the sample canister during the terminal rendezvous phase (< 5 km) of the capture.

The identification of a retroreflector configuration relies extensively on Monte Carlo simulations. Computer simulations show that a spherical t-design yields a strong return for a 50 retroreflectors constellation. The return is calculated utilizing formulas for Rayleigh-Sommerfeld diffraction, and integrating over the surfaces of the retroreflector apertures for the specific orientation of the spherical container. At a distance of 5 km, in simulation the chosen configuration produces a return signal that is at least 5% of the return of a single retroreflector head-on approximately 99.99% of the time. On average, the return signal is 1.36 times the signal of a single retroreflector head-on. The results of the model and empirical results collected at a shorter distance are consistent.

TABLE OF CONTENTS

1. INTRODUCTION
2. INDIVIDUAL RETROREFLECTORS
3. INTERFERENCE OF RETROREFLECTORS
4. SIMULATING DIFFRACTION AND INTERFERENCE
5. VERIFICATION OF SIMULATION TECHNIQUE
6. EVALUATION CRITERION
7. CONSTRAINTS ON RETROREFLECTOR PLACEMENT
8. PRINCIPLES FOR GENERATING A CONFIGURATION
9. FINAL RETROREFLECTOR CONFIGURATION
10. RESULTS OF SIMULATIONS
11. SUMMARY
12. ACKNOWLEDGEMENTS
REFERENCES
APPENDIX A

1. INTRODUCTION

A future Mars mission will return a sample of Martian soil to Earth for further analysis. In one mission concept, the sample will be placed in a spherical container of radius 8 cm, and sent into orbit around Mars. A rendezvous spacecraft will then capture the container and return it to Earth [1].

Coarse, long range location of the sample container will be accomplished using a solar-powered radio beacon. However, final detection and orbit maneuvers will require position knowledge beyond the capabilities of the radio beacon scheme. Accordingly, a laser radar is baselined as the close-approach rendezvous sensor. To increase the laser radar's signal return, retroreflectors will be placed on the surface of the sample container in spaces not occupied by solar cells. In addition to improved accuracy at short range, a second advantage of the laser radar is that it will continue to operate during the 40% of each orbit when the radio beacon is not powered because Mars occludes the sun.

This work focuses on the placement of the retroreflectors to improve the returned signal. In particular, the number, distribution, and orientation of the retroreflectors must assure coverage of the entire 4π solid angle to insure that the orbiting sample canister can be acquired at 5 km. Such coverage essentially demands that, for some set of orientations, more than one retro will contribute to the return signal. If the laser light is coherent, these multiple returns will give rise to interference effects. Small changes in the relative position and orientation of the sample canister with respect to the laser radar may produce large variations in the returned signal. To increase the probability of quickly locating the container, the retroreflectors must be placed so as to maximize the minimum signal returned in any orientation. The placement problem is complicated since the locations of the retroreflectors are limited to areas not occupied by solar cells, radio antennae, etc. The methodology used to optimize the return under these constraints is discussed.

Our approach to identifying optimal retroreflector configurations relies heavily on computer simulations. A plausible retroreflector configuration, constrained by predefined locations of solar cells, radio antennas, etc. is

identified. We then simulate the electromagnetic field from individual retroreflectors, taking into account variables such as distance, shape of the retroreflector aperture, observation angle, and Gaussian beam profile. These individual fields are summed to produce the final interference pattern.

We will present simulations of the interference pattern from a promising retroreflector configuration with illustrations. Monte Carlo simulations of the distribution of the returned signal are also shown. A physical model of the sample container with retroreflectors has also been constructed. Measurements of the return from the physical model have not yet been obtained. However, in section 5, we present measurements of a simplified physical model to validate our technique.

2. INDIVIDUAL RETROREFLECTORS

When the detector is collocated with the light source, the best method of returning light to the detector is to use a retroreflective target such as a corner cube. Corner cubes are made of three adjoining reflecting sides arranged at right angles to one another. When a light ray is incident on one of the three adjoining sides, the ray is reflected to the second side, then to the third, and then back in the direction of the light source. Unlike a mirror, this is true independent of the angle between the light source and the corner cube. A corner cube in which the space between the adjoining sides has been filled with a transparent medium is called a closed corner cube. The advantage of using a closed design as opposed to an open one is that in the closed design, refraction provides a larger acceptance angle.

Corner cubes can have various aperture shapes ranging from triangular to circular. A corner cube with a circular aperture is often produced by cutting the corner cube from a cylinder of glass.

Eckhart (1971) presents a simple model of corner cube reflectance based on calculating the effective apertures of corner cubes of various geometries. The model highlights the differences between cylindrical and triangular reflectors, the effects of tilting a reflector at various angles, and the effects of the index of refraction in retroreflector designs.

In the simplest version of Eckhardt's model, the return signal is proportional to the area of the effective aperture of the corner cube. His paper presents a construction that allows calculation of the effective aperture. In this construction, the corner cube is modeled as two apertures, an entry aperture and an exit aperture. The entry aperture has the same geometry as the actual retroreflector aperture. The exit aperture also has the same size and shape except that it is inverted as shown in figure 1. The two aperture shapes are centered on the principal axis of the corner cube and are separated by a distance of twice the corner cube

height². The effective aperture of a corner cube is the geometrical area of the intersection of the entry and exit apertures projected in the direction of the light source onto a plane normal to that direction.

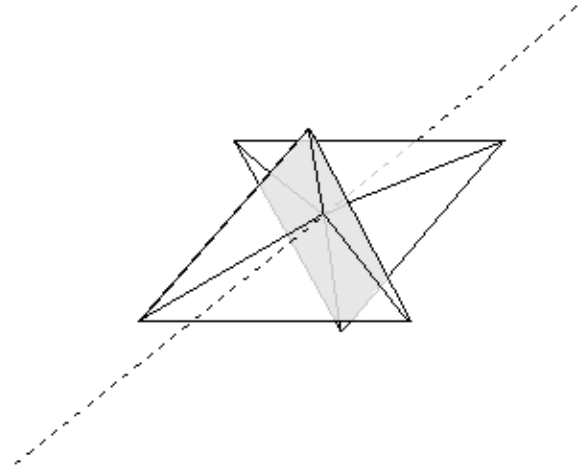


Figure 1. Sketch of Eckhardt's effective aperture construction

If the light source lies on the principal axis of the corner cube, the effective aperture is maximized. However, if the beam enters at an angle, two effects cause the effective aperture to decrease in size. First, the entry and exit apertures are foreshortened by the observation angle so as to decrease the effective area of each. Second, the centers of the two apertures are offset with respect to each other. This serves to diminish the size of the intersection.

To take into account the effect of the index of refraction, the direction of projection of the two apertures is taken as the direction of propagation of the transmitted beam through the corner cube material. This direction may be calculated using Snell's Law:

$$\sin q_t = \frac{1}{n} \sin q_i \quad (1)$$

In this equation, ϑ_i denotes the angle of the incident ray with the glass face of the corner cube; ϑ_t denotes the angle of the ray transmitted through the corner cube material; n is the index of refraction.

In a closed design, the effect of foreshortening is the same as in an open design. However, the effect of the offset of the center points is diminished.

A second effect of the index of refraction is the loss at entry and exit surfaces due to reflection. These losses are calculated using the Fresnel equations for unpolarized light:

² The height of a retroreflector is the distance from the point of convergence of the three mirrored surfaces to the aperture face along the principal axis.

$$R = \frac{1}{2} \left[\frac{\sin^2(\mathbf{q}_t - \mathbf{q}_i)}{\sin^2(\mathbf{q}_t + \mathbf{q}_i)} + \frac{\tan^2(\mathbf{q}_t - \mathbf{q}_i)}{\tan^2(\mathbf{q}_t + \mathbf{q}_i)} \right] \quad (2)$$

R is the proportion of light lost due to reflectance at the corner cube surface. This equation must be applied twice, upon entry and exit of the ray from the corner cube.

Figure 2 graphs the effective aperture of three different corner cube designs calculated using this geometrical method. The figure plots the effective aperture of an open triangular corner cube, an open cylindrical corner cube, and a closed cylindrical corner cube with index of refraction 1.52. Along the x-axis, we vary the angle of incidence of the light. The y-axis plots the effective aperture (including the loss due to reflection for the closed cube design), which by this model is proportional to the total flux returned from the retroreflector in the direction of the light source.

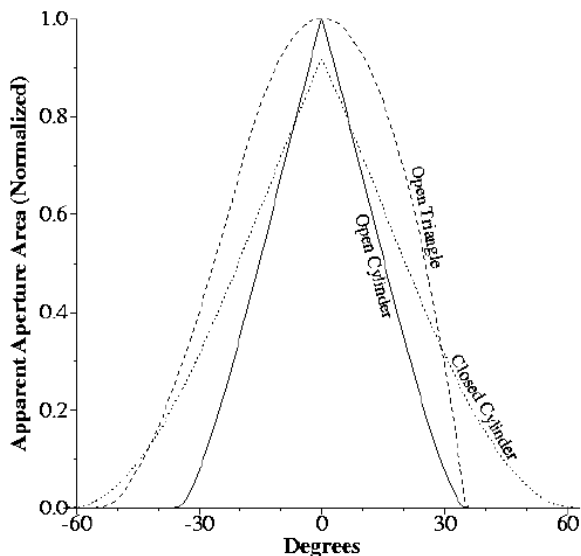


Figure 2. The effective aperture for three different corner cube designs

The sizes of the three retroreflectors are chosen to have the same head-on effective aperture area. This means that the height of the two cylindrical designs is larger than the triangular design by a factor of 1.05.

An open cylinder corner cube is an open triangle with the corners cut off. Comparing the open cylinder and open triangle curves in figure 2 shows that the corners of the triangle are useful in increasing the return at most angles.

Comparing the open and closed cylinder curves demonstrates the combined effect of reflection and refraction. At zero degrees, the effect of reflection shows up as an 8% loss in the closed design. However, the loss due to reflection is quickly overcome by the advantage of refraction as the angle increases.

As the figure shows, the closed cylinder produces the largest return of the three designs at large angles. The use of antireflective coatings on the closed cylinder design would cancel much of the effect of reflection, and increase the height of the curve along most of its extent. Another advantage of the cylindrical design is that less surface area on the sphere is required by this geometry. For these reasons, we have chosen the cylindrical retroreflector design for use in this work.

Figure 3 below shows an image of the retroreflector that is baselined for this study. It is a cylindrical design with a circular aperture with diameter of 7.16 mm, a height of 6.1 mm. It has silvered reflecting surfaces, but no antireflective coatings. The medium is BK7 glass.

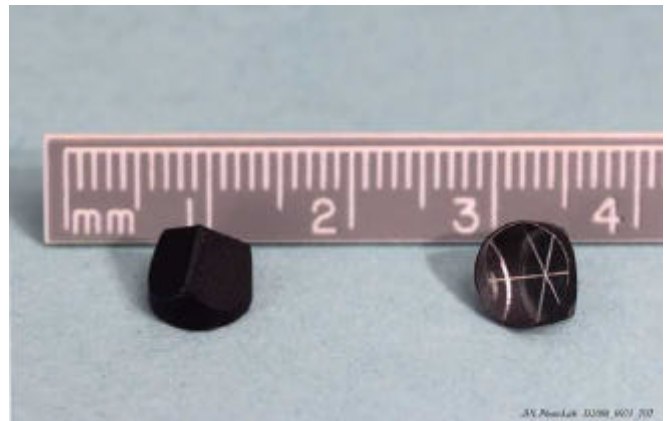


Figure 3. Image of retroreflectors used in this work

There are a number of corner cube phenomena that are not accounted for by such a simple geometric model – for example, the effect of non-uniform illumination from the Gaussian beam at short distances, the effect of diffraction at long distances³, and the effect of interference between retroreflectors. In section 3, we will discuss the interference generated by multiply illuminated retroreflectors. The solution for modeling the interference effect, discussed in section 4, will also end up solving these other shortcomings as well.

3. INTERFERENCE OF RETROREFLECTORS

Laser light is used to illuminate the sample sphere. Because laser light is coherent, interference phenomena can occur. Initially, laser light returned from a single retroreflector head-on is shown in figure 4. In this simulation, the retroreflector is 5 km away from the laser radar, the wavelength of the laser is 1064 nm, and the size of the figure covers an area of 1.6m x 1.6m. Most laser radars have shared optics for the receiver and transmitter. Therefore, it has been assumed in this work that the spatial positions of the receiver and transmitter are the same. The detector is located in the center of the image, and has a square

³ Eckhardt is aware of the problem of diffraction, and suggests a method for adjusting for it. His method is different from the method used in this study.

collecting aperture of 5 cm side length. It is observed in figure 4 that, due to diffraction, the return from the retroreflector is smeared out over approximately 1 meter. Without diffraction, the diameter of the signal would be about 1.4 cm, as calculated using pure geometric optics.

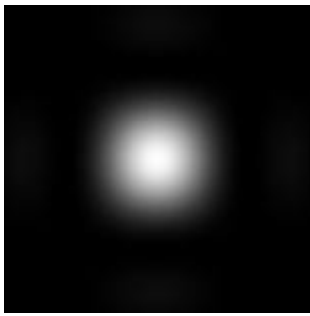


Figure 4. The returned signal from a single retroreflector

Due to interference, the returned signal is very different when the laser beam hits two retroreflectors. Figure 5 shows a simulation of the returned signal from 2 similar retroreflectors that are placed 4 cm apart at 5 km. The rest of the conditions are the same as in figure 4.

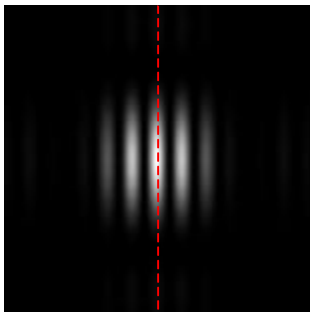


Figure 5. The returned signal from two retroreflectors. The dotted line indicates center of image

It is observed in figure 5, that the signal is very bright in the center of the image. This is where the detector is located. The intensity of light in this position is more than twice that of a single retroreflector. The effect of interference in this case is to augment the return signal beyond that which is expected from two reflectors.

In our capture scenario, the sample canister is likely to be spinning in orbit around Mars. Hence, the retroreflectors will be moving relative to each other. If one retroreflector in a pair moves closer to the light source by a quarter of a wavelength of light, the resulting fringe pattern will shift by half a fringe width leaving the detector in a dark band. This scenario is shown in figure 6. Note that there is little or no returned signal in the center of the image.

The fringe patterns discussed so far have all been one-dimensional. This is not the case when the signal is returned from a two dimensional constellation of retroreflectors. In that case, the fringe pattern will also be 2 dimensional. As an example, figure 7 shows the return from 3 retroreflectors

placed in an equilateral triangle with sides of 3.46 cm. Figure 8 shows the return from 4 retroreflectors placed in a square with sides of 4 cm. All other conditions are the same as in the previous examples.

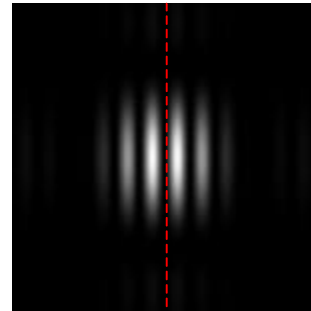


Figure 6. The returned signal from two retroreflectors that are displaced a quarter of a wavelength relative to each other. The dotted line indicates center of image

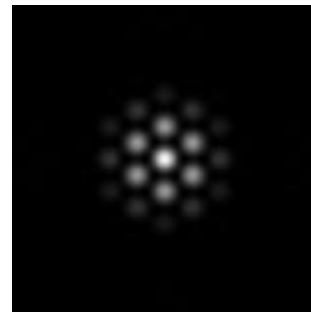


Figure 7. The returned signal from 3 retroreflectors

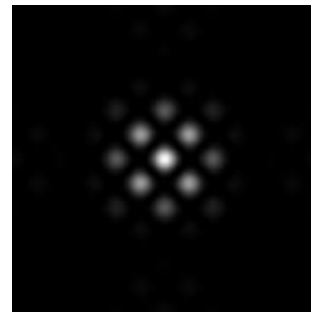


Figure 8. The returned signal from 4 retroreflectors

4. SIMULATING DIFFRACTION AND INTERFERENCE

In our simulation, we propagate the light from a point source⁴ (the laser) forward to the corner cube aperture plane, represented by a field of complex values. This field is then propagated back to the plane of the detector, which is represented as another field of complex values. Each corner

⁴ The change in intensity across the face of the corner cube aperture is simulated as if produced by the Gaussian beam of the laser. However, the distance any light ray must travel is calculated as if it originated at a point source.

cube produces such a field at the detector. The aggregate return signal of all the corner cubes can be found by adding together all of these detector complex fields.

Figure 9 illustrates this process. A ray originating at the laser at point P_0 , propagates through an aperture at some point P_1 , and arrives at the detector at point P_2 . When the aperture is a corner cube, the light ray exits the aperture in the opposite direction from which it entered. The formulation we present here is quite general. For simplicity, we have unfolded the path of the ray in figure 9.

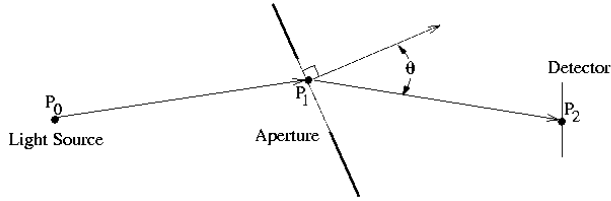


Figure 9. Light propagates from the source to the detector via the corner cube aperture

The propagation of light from the point source P_0 to some point P_1 in the aperture proceeds according to the following equation:

$$U(P_1) = \frac{a}{\|P_1 - P_0\|} e^{i\frac{2\pi}{\lambda}\|P_1 - P_0\|} \quad (3)$$

$U(P_1)$ is a complex number representing the amplitude and phase of the signal at position P_1 ; a is the amplitude of the light at unit distance from the source; λ is the wavelength of the laser. As the distance $\|P_1 - P_0\|$ from P_0 to P_1 increases, the amplitude of $U(P_1)$ decreases. The distance also determines the phase of $U(P_1)$.

The propagation of light from the aperture to the detector proceeds according to the Rayleigh-Sommerfeld diffraction formula given below[3]:

$$U(P_2) = \iint_{P_1 \in S} \frac{\cos \mathbf{q}}{\|P_2 - P_1\|} e^{i\frac{2\pi}{\lambda}\|P_2 - P_1\|} U(P_1) dS \quad (4)$$

The integral covers all points P_1 within the two-dimensional area of the aperture S whose shape is determined using Eckhardt's methodology; \mathbf{q} is the angle that the exiting ray makes with the aperture normal. When light passes through several apertures (corner cubes) in parallel on the way to the detector, the integral is performed across the areas of all of them. In our implementation, the points P_1 are sampled in a regular grid across each aperture. The integral is thus approximated by a summation.

The intensity of the signal is calculated as:

$$I(P_2) = U(P_2) \cdot \overline{U(P_2)} \quad (5)$$

$\overline{U(P_2)}$ is the complex conjugate of $U(P_2)$. $I(P_2)$ is a scalar value representing the intensity of the signal at some point P_2 on the detector. Each intensity value reported later in this paper is the sum of the intensities for all points P_2 on the detector.

5. VERIFICATION OF SIMULATION TECHNIQUE

A laboratory experiment was performed to verify the described model. We built a small constellation of three retroreflectors. The reflectors were pointed in the same direction and placed at the corners of an equilateral triangle with distance between centers of 11.3 mm. A 650-nm laser pointer was directed at this target from 60 meters away. The light from the laser pointer passed through a beam splitter on its way to the retroreflectors. On its way back, a portion of the return signal was deflected by the beam splitter onto a projection screen where an image of the return signal formed. A sketch of the setup is shown in figure 10. A CCD camera was pointed at the projection screen and acquired images.

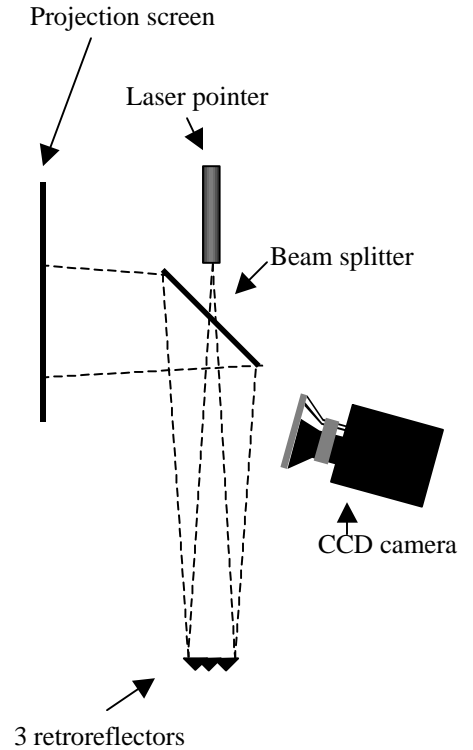


Figure 10. Sketch of the laboratory experiment. The distance between the retroreflectors and the beam splitter is about 60 meters

The image acquired with the CCD camera was compared to the results of the model. The predicted return by the model is shown in figure 11 and the image from the CCD camera is shown in figure 12. It is observed that the model and the calculated return are very similar both in size and shape.

The reason for the slight warping of the CCD image is because the three retroreflectors were mounted at an angle on a tripod. The blurring of the CCD image may be due to a number of differences between the simulation and the real world situation: a difference in alignment between the beam and the three retroreflectors, polarization effects, mechanical shifts, atmospheric turbulence, and long exposure time. Further testing is required to completely validate the model. However these results suggest the model captures the major physical effects.

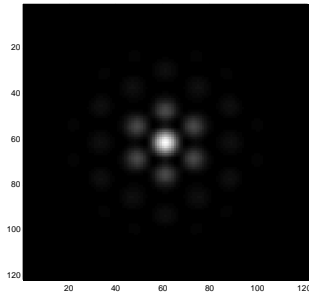


Figure 11. The prediction of the model for the laboratory experiment. The figure covers an area of 3 cm by 3 cm

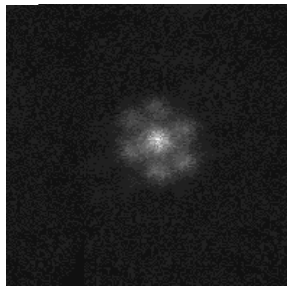


Figure 12. Image acquired with the CCD camera. The figure covers an area of 3 cm by 3 cm

6. EVALUATION CRITERION

As the sample canister rotates in space, the distances to the various retroreflectors will continually change, resulting in changes in the pattern of dark and light areas at the detector. If the distance between these bands is large enough, a small sensor will sometimes be completely covered by a bright fringe, and sometimes by a dark fringe. Therefore, we should expect large variations in the intensity of the return signal due to the spinning of the sample canister, and other movements.

In the case where the distance to the sample canister is large, the average return signal may be small, perhaps near the detection limit of the sensor. If the precise angular position of the sample canister is known, this is not a problem. We can send a large number of laser pulses, and even though some of the returns will be below the detection limit, as the sphere rotates, eventually we will get a return that is large enough to detect.

This approach is not viable for the initial acquisition of the target with the scanning laser system at 5 km. During acquisition, it may be necessary to scan a large area of space. Since the spacecraft and the sample canister are moving with respect to each other, there may not be time to do multiple scans. The acquisition conditions set the criterion we use to evaluate a retroreflector configuration. Therefore we seek a configuration of retroreflectors which maximizes the probability that the canister will be detected with a single pulse at 5 km.

The parameters of the laser radar have not yet been finalized, so we do not know the minimum detection threshold of the sensor. To deal with this situation, we arbitrarily set the detection threshold at 5 percent of the expected return from a single retroreflector head-on at a distance of 5 kilometers. The best retroreflector configuration is the one that maximizes the probability of detection across all possible orientations of the canister.

7. CONSTRAINTS ON RETROREFLECTOR PLACEMENT

The placement of corner cubes on the surface of the sphere is constrained in two ways. First, we are constrained by where we are allowed to place corner cubes on the surface of the sphere. Certain areas are reserved for solar cells to power the radio beacon, for antennas, the lid etc. Tentatively, it has been decided that there is room for as many as 50 retroreflectors, one retroreflector on each pole and 4 bands located at latitudes of -36° , -11° , 11° and 36° . Each band contains room for 12 equally spaced retroreflectors.

Second, we are limited in the amount of tilt we can place on each retroreflector. As shown in figure 13, tilting a retroreflector from the normal orientation increases the surface area required to contain it. No retroreflector is allowed to protrude above the sphere surface. Therefore, applying a tilt means the retroreflector must be inset below the surface. A recess in the shape of a funnel must be created in the surface in order to avoid obstructing the viewing angle. Because the surface space reserved for each retroreflector is limited, this places a constraint on how much tilt we can apply to any retroreflector.

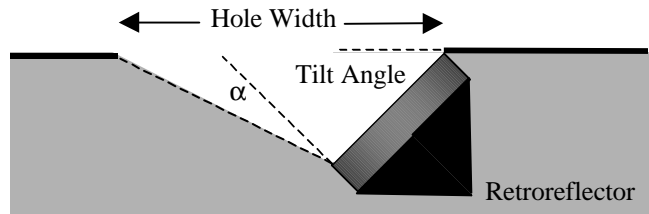


Figure 13. A retroreflector recessed below the surface

Figure 14 graphs the diameter of the hole required to accommodate a retroreflector that is tilted at various angles. The required viewing angle in degrees is denoted α in this plot, and in figure 13. There is a separate curve plotted for

each required viewing angle α . The corner cubes we use for this study have a maximum viewing angle of 55° off axis. Because the diameter increases very quickly above 25° we have set a maximum of 25° tilt on any retroreflector.

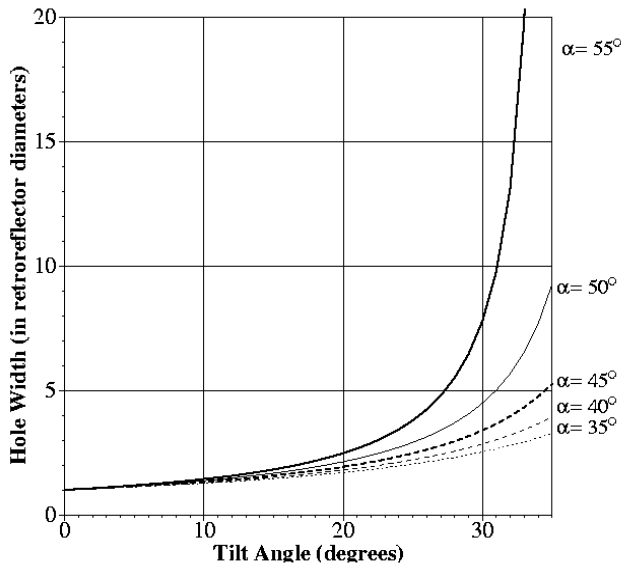


Figure 14. The diameter of the hole required to accommodate a recessed retroreflector tilted at various angles

8. PRINCIPLES FOR GENERATING A CONFIGURATION

The electromagnetic field simulation technique is slow. Rather than use this technique to evaluate every conceivable retroreflector configuration, our approach has been to apply some guiding principles to produce good configurations, and then evaluate them using the electromagnetic field simulation. In the following sections, we discuss three guiding principles we have used.

8.1 CORNER CUBES SHOULD EVENLY COVER ALL SKY ANGLES

Clearly we should not have any patches of sky towards which no retroreflectors point. This leads to the first guiding principle – retroreflectors should be oriented to evenly cover all viewing angles. One can recast this in terms of locating points on a spherical surface.

There exist a number mathematical theories for placing 50 points optimally on a unit sphere. [5]:

1). Spherical coverings: Minimize the maximum distance from any point on the sphere to its nearest neighbor. In the context of retroreflectors, “distance” translates into angle of incidence, hence minimizing the maximum distance between two points minimizes the maximum angle of incidence of the sphere’s retroreflectors. The desirability of

so doing is suggested by figure 2. The optimal constellation utilizing this approach is shown graphically in figure 15.

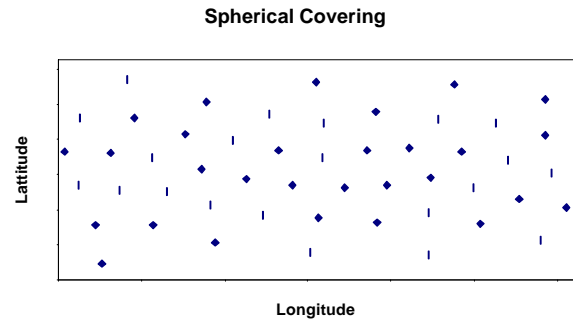


Figure 15. The 50 retroreflector spherical covering constellation

2). Spherical codes: Maximize the minimum distance between any two retroreflectors. The optimal constellation utilizing this approach is shown in figure 16.

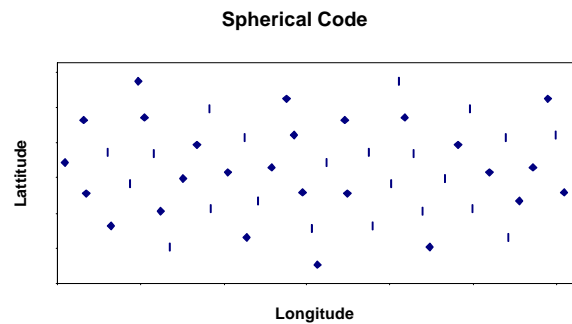


Figure 16. The 50 retroreflector spherical code constellation

3). Spherical t-design: This approach places 50 points on a sphere so as to perfectly reproduce the integral across the surface of the sphere of any polynomial function with degree t, where t is as large as possible. The optimal constellation utilizing this approach is shown graphically in figure 17.

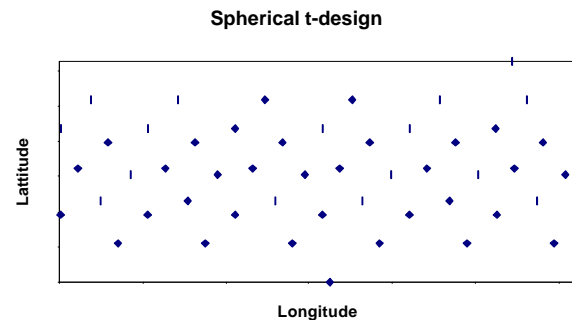


Figure 17. The 50 retroreflector spherical t-design constellation

4). Minimal Energy: Place 50 retroreflectors on a sphere with minimal potential ($\sum_{ij} 1/||p_i-p_j||$). The optimal constellation utilizing this approach is shown graphically in figure 18.

Minimal Energy Arrangement

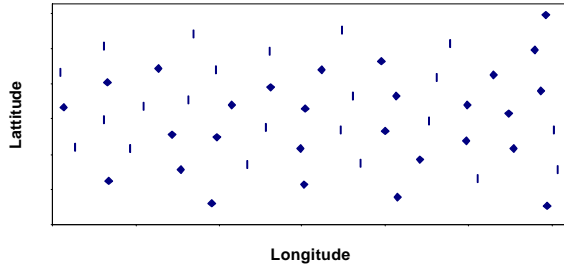


Figure 18. The 50 retroreflector minimal energy constellation

5). Maximum volume spherical codes: Maximize the volume of the convex hull. The optimal constellation utilizing this approach is shown graphically in figure 19.

Maximum Volume

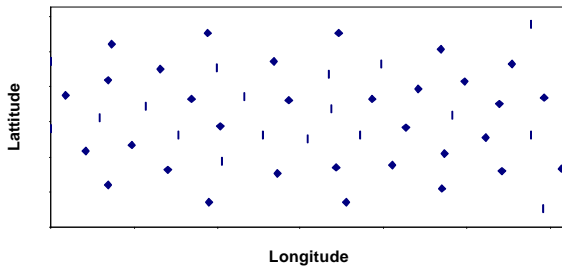


Figure 19. The 50 retroreflector maximum volume constellation

It is too complex to analytically choose the optimal constellation. Also, the simulation technique outlined in section 3 is very time consuming. Therefore, instead of using either of these techniques, we chose the constellation using a simple Monte Carlo evaluation function. For each constellation, we generated 100,000 randomly selected orientations, and estimated the resulting return signal. The return of each individual retroreflector was determined using the geometrical approach outlined in section 2. The sum of these, ignoring interference, is then used as the aggregate return from the constellation in this orientation. It is observed in table 1 that the returned signal varies by only a few percent. The Spherical t-design was among the best constellations, and it was selected for further study. It is likely, that the Spherical Code (or other constellations) would have performed similar or marginally better.

Table 1. Minimum return for the different constellations

Constellation	Min return (1 = single retroreflector head-on)
Spherical Covering	2.69
Spherical Code	2.78
Spherical t-design	2.76
Minimal energy	2.75
Maximum volume	2.62

8.2 INCREASE TOTAL EFFECTIVE APERTURE

The second guiding principle is fairly intuitive. If we increase the total effective aperture of the corner cubes, either by increasing the number of corner cubes or by increasing the size of each corner cube, it will increase the size of the average return signal.

It is important to keep in mind that, even though interference produces dark fringes, no light is ever lost in this process. Rather, the total flux from the corner cubes is merely redistributed spatially from the dark fringe areas to create the brighter areas. Our goal is not to increase the average return signal, but to maximize the probability of getting a return that is higher than our threshold. However, increasing the average signal tends to increase this probability as well.

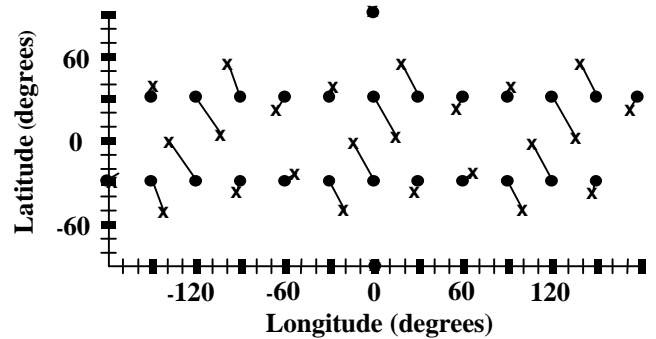


Figure 20. The 26 retroreflector spherical t-design constellation

The following sequence of images illustrates the first two guiding principles. Figure 20 shows the spherical t-design constellation for 26 retroreflectors. To satisfy the constraints imposed by the placement of solar cells, etc. in one design of the sample canister, the retroreflectors were mapped onto 2 bands of 12 at $\pm 30^\circ$, plus a retro at each pole as shown in the figure. Each such open position is marked by a \bullet in the figure. Each x marks the position of a retroreflector specified by the spherical t-design were it placed so that it were normal to the surface. The lines in the figure specify which surface normal corresponds to which open position in the final placement. A retroreflector is placed in the position specified by the \bullet , while maintaining the orientation specified by the x . Longer lines in the figure indicate a larger tilt from surface normal.

Figure 21 shows the intensity of the return signal from this constellation at all points on the sky. This image was created using the simulation technique of section 4 to perform 30,000 random orientations of the constellation. Bilinear interpolation was used to generate the pixel values. This causes the granularity at the poles to be larger. Notice that the bright spots in the image correspond to the x s in figure 20. In other words, the brightest spots occur at where the retroreflectors are pointing, while the dark spots (and the majority of the returns less than our 5% threshold) occur in the spaces between where the retroreflectors are pointing.

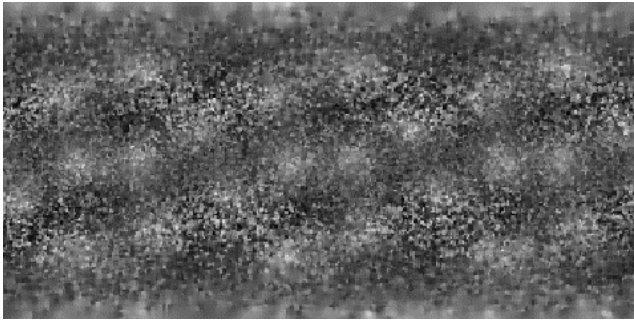


Figure 21. The 4δ steradians return signal for the constellation of figure 20. The x-axis is longitude and the y-axis is latitude.

Figure 22 shows the 50 retroreflector spherical t-design constellation using a sample canister design which adds two more bands. Figure 23 maps the return signals. Figures 21 and 23 have both been normalized to a brightness that is best for viewing. The average return of the 50 retroreflector design is actually $50/26$ times brighter than the 26 retroreflector design. This illustrates guiding principle 2 – more total aperture is better.

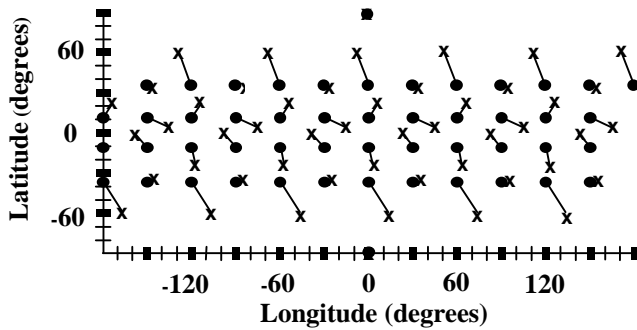


Figure 22. The 50 retroreflector spherical t-design constellation

Notice that in figure 23 the regular variations in intensity have disappeared. This is a demonstration of the first guiding principle. Every part of the sky is covered smoothly by one or more reflectors, so the dips between retroreflectors have been smoothed out. We could also have increased the total effective aperture (guiding principle 2) by increasing the size of each retroreflector in the 26 retroreflector configuration. By doing this, we could have achieved a similar increase in average return. However, by increasing the number of retroreflectors instead, we were able to apply both of the first two guiding principles, and produce a better design.

Despite the fact that the regular dips have been removed with this design, there remains significant speckle in figure 23. The speckle results from interference from multiple corner cubes. If the speckle could be removed, the return from every orientation would equal the average return. In our application, this would be large enough to allow detection from any orientation. Unfortunately, we are

unaware of any way to completely remove the speckle. However, as discussed in the next section, a third guiding principle suggests one way to reduce it.

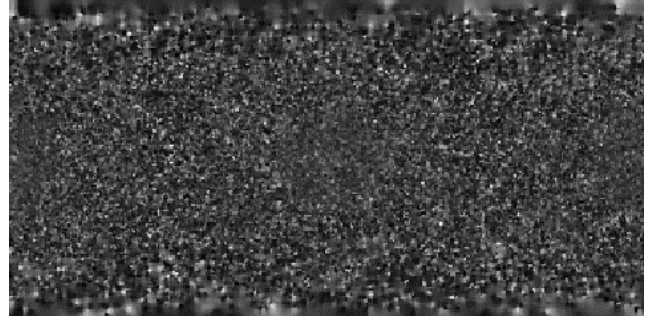


Figure 23. The full-sky return signal for the constellation of figure 22.

8.3 SEPARATE CORNER CUBES THAT COVER SIMILAR VIEWING ANGLES

In section 3, we set up a situation in which two retroreflectors were mounted side by side at a distance of 5 km from the laser range finder. We demonstrated that moving one of the reflectors one quarter of a wavelength of light toward the laser/sensor resulted in shifting the fringe pattern by one half fringe. This shifting may move the detector from a bright band to a dark band.

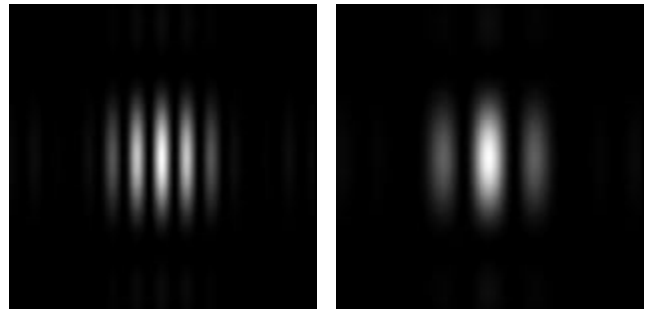


Figure 24. The effect of moving two retroreflectors closer together

Figure 24 demonstrates what happens when we move the two retroreflectors closer together. On the left, a distance of 4 cm separates the two reflectors, just as in figure 5. On the right, the reflectors have been moved closer together, so that they are separated by 2 cm. The result is that the bands in the fringe pattern are now much wider. If the retroreflectors are far enough away to be considered point sources, this observation may be quantified by the following equation. [4].

$$\Delta y \approx \frac{s \cdot l}{a} \quad (6)$$

Here, Δy is the fringe width, s is the distance from the laser radar to the reflectors, a is the distance between the reflectors, and l is the wavelength.

If the band pattern were narrower than the detector width, the return signal would vary very little. It would always be near the average. Since our goal is to increase the minimum return signal, a narrow band pattern, and thus maximally separated reflectors, is to be preferred.

This demonstrates a third general principle which may be helpful in improving the return signal – any pair of retroreflectors which point to the same part of the sky should be separated spatially as much as possible.

As we have seen earlier, retroreflectors do not have to be oriented normal to the surface of the spherical sample container. They can be mounted at an angle. Ideally, we would choose the positions of the reflectors on the surface of the sphere to create the largest possible spatial separation between retroreflectors which point to the same part of the sky.

In our current scenario, general principle 3 cannot be effectively applied. As discussed in section 7, we have a requirement that no reflector be moved more than 25° from its surface normal position. This constraint, along with the sparseness of the positions open for placement of retroreflectors allow too little leeway to apply this general principle.

9. FINAL RETROREFLECTOR CONFIGURATION

The design described by figure 22 was chosen as the basis for a physical model. This model has been constructed in nylon with small aluminum insets to hold the retroreflectors. A picture of the model is shown in figure 25. To avoid grinding funnel-shaped holes, the sphere was given a radius of 7 cm. The aluminum insets protrude 1 cm beyond the surface to simulate a sphere of radius 8 cm. The return signal from the model has not yet been characterized empirically.

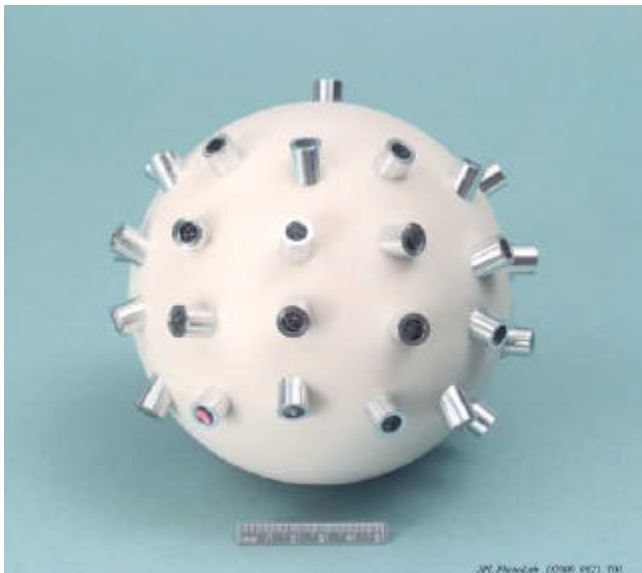


Figure 25. Picture of the physical model

10. RESULTS OF SIMULATIONS

The configuration of the physical model has been simulated using the simulation techniques outlined in section 4. A typical return from a random orientation of the sphere is shown in figure 26. The figure covers an area of 1.6m by 1.6m.

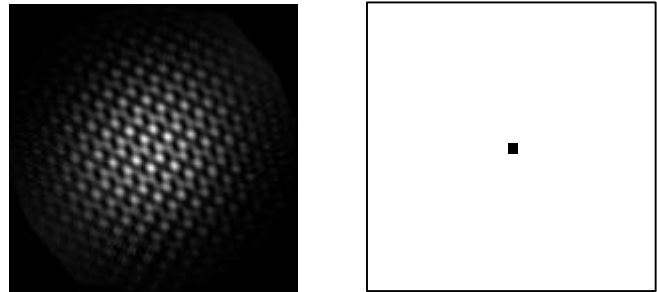


Figure 26. Returned signal intensity from a random orientation of the sphere. The small square beside the image represents the size of the detector.

In order to calculate the probability distribution of the signal strength, this simulation was reiterated 30,000 times with random orientations of the sphere. The resulting distribution is shown in figure 27. The unit of the x-axis is the signal strength relative to a single retroreflector head-on. The unit of the y-axis is probability. The average signal strength is 1.36 times the return of a single reflector head-on. There was only one instance out of 30,000 in which the signal strength dipped below 5% of the signal of a single reflector.

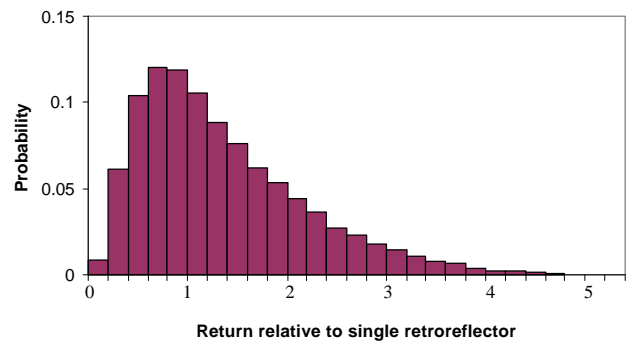


Figure 27. Histogram of signal strength

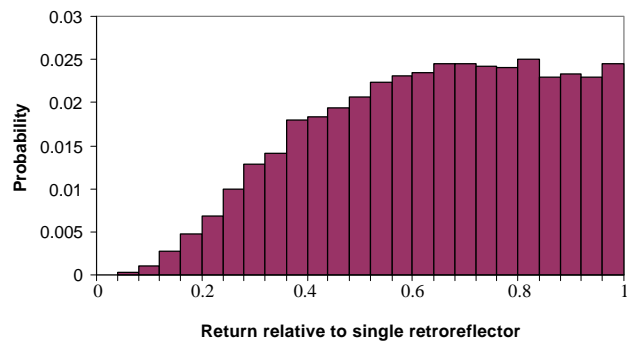


Figure 28. Detail of small signal tail of figure 27

The strength of this one instance was 4.5%. Because the bottom tail of this curve is most important, we also present an expanded view of the low-strength region of this distribution in figure 28.

11. SUMMARY

In this work, a model of a sphere studded with retroreflectors has been constructed. The objective of the work is to identify a configuration of retroreflector positions/orientations on a sphere that will maximize the return from a laser radar at a distance of 5 km. A simulation of the interference of multiple light sources was developed based on the Rayleigh-Sommerfeld diffraction formula, and on a geometrical model of corner cube effective aperture due to Eckhardt. Due to mechanical constraints, a 50-point retroreflector configuration was chosen. Numerical simulations showed a so-called spherical t-design produced a good return. Simulations have provided the intensity profile and spatial distributions of returns. In simulation, the chosen constellation produced an average signal strength of 1.36 times that of a single retroreflector head-on, and a return of at least 5% of the single reflector signal more than 99.99% of the time.

12. ACKNOWLEDGEMENTS

The research described in this paper was carried out at the Jet Propulsion Laboratory, California Institute of Technology, under a contract with the National Aeronautics and Space Administration. Reference herein to any specific commercial product, process or service by trademark, manufacturer, or otherwise, does not constitute or imply its endorsement by the United States Government or the Jet Propulsion Laboratory, California Institute of Technology.

REFERENCES

- [1] O'Neil, William; Cazaux, Christian (1999): The Mars Sample Return Project, IAF, International Astronautical Congress, 50th, Amsterdam, Netherlands, Oct. 4-8, 1999, IAF Paper 99-Q302.
- [2] H. D. Eckhardt (1971): *Simple Model of Corner Reflector Phenomena*. *Applied Optics*, **10**:7, 1559-1566.
- [3] Joseph W. Goodman (1968): *Introduction to Fourier Optics*. McGraw-Hill.
- [4] Eugene Hecht (1998): *Optics*, 3rd Edition. Addison-Wesley Pub Co; ISBN: 0201838877.
- [5] R. H. Hardin, N. J. A. Sloane and W. D. Smith, Tables of spherical codes with icosahedral symmetry, published electronically at:
<http://www.research.att.com/~njas/icosahedral.codes/>.

Dr. Daniel Clouse received the B.A. degree in computer science from the University of California, Berkeley in 1982, the M.S. degree in computer science from the University of California, San Diego (UCSD) in 1992, and the Ph.D. degree in cognitive science and computer science from UCSD in 1998. He is a staff member at the Jet Propulsion Laboratory, California Institute of Technology in the Machine Vision group of the Autonomy and Control Section. His interests include vision processing, neural networks, language translation, and word sense disambiguation.



Dr. Carl Christian Liebe received the M.S.E.E. degree in 1991 and the Ph.D. degree in 1994 from the Department of Electrophysics, Technical University of Denmark. Since 1997, he has been staff at the Jet Propulsion Laboratory, California Institute of Technology. His current research interests are new technologies and applications for autonomous attitude determination. He has authored/co-authored more than 30 papers.



Dr. Curtis Padgett received his Ph.D. from the Computer Science and Engineering Department at the University of California at San Diego (UCSD) in 1998. He received his M.S. degree from the same department in 1992. He has been employed at the Jet Propulsion Laboratory, California Institute of Technology, Pasadena since 1993. He is a Senior Member of the Technical Staff in the Machine Vision group of the Autonomy and Control Section where he works on remote sensing applications for space systems. His research interests include algorithm optimization, machine vision, and artificial intelligence applied in classification and pattern recognition tasks.



Randy Bartman received a B.S. degree in physics from California Institute of Technology in 1976, and joined the Jet Propulsion Laboratory shortly thereafter. He is currently deputy section manager for the Interferometry Systems and Technology Section. His research interests include lasers, active optical sensors, and interferometry.



APPENDIX A

The following coordinates were used for the retroreflector physical model. The sphere has a radius of 7 cm. The Cartesian coordinates for the line segments defining 50 holes are shown below. A pipe is fitted in each hole. The retroreflector is at the end of the pipe at a radial distance of 8 cm.

Column 1: x coordinate of point on sphere surface
 Column 2: y coordinate of point on sphere surface
 Column 3: z coordinate of point on sphere surface
 Column 4: x coordinate of end point inside the sphere
 Column 5: y coordinate of end point inside the sphere
 Column 6: z coordinate of end point inside the sphere

The units are in cm.

0.0000	0.0000	7.0000	0.0000	0.0000	5.0000
5.6523	-0.0447	4.1292	4.0149	-0.1339	2.9842
5.0811	3.0056	3.7615	4.1299	2.5872	2.0527
2.8648	4.8726	4.1292	2.1234	3.4100	2.9842
-0.0623	5.9032	3.7614	-0.1755	4.8702	2.0526
-2.7875	4.9173	4.1292	-1.8915	3.5439	2.9842
-5.1434	2.8977	3.7615	-4.3054	2.2833	2.0527
-5.6523	0.0447	4.1292	-4.0149	0.1339	2.9842
-5.0811	-3.0056	3.7615	-4.1299	-2.5872	2.0527
-2.8648	-4.8726	4.1292	-2.1234	-3.4100	2.9842
0.0623	-5.9032	3.7614	0.1755	-4.8702	2.0526
2.7875	-4.9173	4.1292	1.8915	-3.5439	2.9842
5.1434	-2.8977	3.7615	4.3054	-2.2833	2.0527
5.6524	-0.0502	-4.1290	4.0158	-0.1504	-2.9840
5.1811	2.8427	-3.7517	4.4195	2.1357	-2.0429
2.8697	4.8699	-4.1290	2.1381	3.4023	-2.9840
0.1289	5.9084	-3.7516	0.3605	4.8954	-2.0428
-2.7828	4.9201	-4.1290	-1.8778	3.5527	-2.9840
-5.0523	3.0658	-3.7517	-4.0593	2.7598	-2.0429
-5.6524	0.0502	-4.1290	-4.0158	0.1504	-2.9840
-5.1811	-2.8427	-3.7517	-4.4195	-2.1357	-2.0429
-2.8697	-4.8699	-4.1290	-2.1381	-3.4023	-2.9840
-0.1289	-5.9084	-3.7516	-0.3605	-4.8954	-2.0428
2.7828	-4.9201	-4.1290	1.8778	-3.5527	-2.9840
5.0523	-3.0658	-3.7517	4.0593	-2.7598	-2.0429
6.8370	-0.2836	1.4746	4.9130	-0.8208	1.3764
6.0315	3.3746	1.1103	4.5437	2.3074	0.3055
3.6642	5.7792	1.4745	3.1676	3.8444	1.3763
0.0933	6.9108	1.1103	0.2737	5.0888	0.3055
-3.1729	6.0629	1.4746	-1.7457	4.6653	1.3764
-5.9383	3.5361	1.1102	-4.2703	2.7813	0.3054
-6.8370	0.2836	1.4746	-4.9130	0.8208	1.3764
-6.0315	-3.3746	1.1103	-4.5437	-2.3074	0.3055
-3.6642	-5.7792	1.4745	-3.1676	-3.8444	1.3763
-0.0933	-6.9108	1.1103	-0.2737	-5.0888	0.3055
3.1729	-6.0629	1.4746	1.7457	-4.6653	1.3764
5.9383	-3.5361	1.1102	4.2703	-2.7813	0.3054
6.8407	0.1599	-1.4760	4.8675	0.4717	-1.3778
5.9931	3.4416	-1.1123	4.4233	2.4994	-0.3075
3.2818	6.0043	-1.4760	2.0252	4.4515	-1.3778
0.0159	6.9110	-1.1124	0.0469	5.0804	-0.3076
-3.5588	5.8443	-1.4760	-2.8422	3.9797	-1.3778
-5.9772	3.4693	-1.1123	-4.3764	2.5809	-0.3075
-6.8407	-0.1599	-1.4760	-4.8675	-0.4717	-1.3778
-5.9931	-3.4416	-1.1123	-4.4233	-2.4994	-0.3075
-3.2818	-6.0043	-1.4760	-2.0252	-4.4515	-1.3778
-0.0159	-6.9110	-1.1124	-0.0469	-5.0804	-0.3076
3.5588	-5.8443	-1.4760	2.8422	-3.9797	-1.3778
5.9772	-3.4693	-1.1123	4.3764	-2.5809	-0.3075
0.0000	0.0000	-7.0000	0.0000	0.0000	-5.0000